

INDOOR AERIAL VEHICLE NAVIGATION USING ULTRA WIDEBAND ACTIVE TWO-WAY RANGING

Brandon Dewberry* and Mike Einhorn†

Precision, robust localization is a key requirement for the safe and effective use of mobile robots. Ultra Wideband (UWB) ranging and communications has been shown to support precision and robust localization indoors and in high multipath venues where GNSS is compromised. Recent research is aimed towards integrating this technology into a variety of unmanned mobile platforms, fusing peer-to-peer ranging into intrinsic recursive optimal localization solutions.

This paper extends this research and demonstrates three-dimensional real-time location and velocity estimation indoors on a small (~2kg) modified multicopter platform. It describes the underlying ranging, network, and navigation processes in detail, pointing out the error sources due to both survey misalignment, range measurement jitter, and geometric dilution of precision (GDOP).

INTRODUCTION

All modern rotorcraft utilize inertial and magnetic measurements for stabilized flight, and these are often coupled with Global Navigation Satellite System (GNSS) positions to provide a full navigation solution and pose estimate. This enables pre-configured flight plans to be loaded into the vehicle controller for automatic execution.

However for indoor operation, during take-off and landing, or where higher precision is required, GNSS alone isn't sufficient. A number of alternatives have been investigated with various capabilities and drawbacks.

For indoor operation most investigators are pursuing various forms of vision and/or LiDAR-based systems coupled with Simultaneous Localization and Mapping (SLAM) techniques. While these techniques are useful, a heavy computational and sensor burden is placed on the vehicle, often coupled with structuring the environment to provide adequate features. The system under study is not at all contrary to SLAM navigation; it simply provides sufficient landmarks for continual correction. Using landmarks limits drift and improves accuracy, which is warranted for many industrial applications if landmark installation is relatively easy.

* Time Domain, 4955 Toney Dr. Huntsville, AL 35802



Figure 1. UWB radio mounted on quadrotor in flight.

Arguably the most capable indoor 3D dynamic localization system is optical motion capture. In this the high-speed images of a number of static cameras are combined to track reflective markers on the vehicle(s). These systems provide excellent accuracy and high update rates. Notable users of these systems include ETH Zurich's Flying Machine Arena [1], and the Kumar Lab at UPENN [2]. While these systems provide a gold standard for dynamic indoor localization, they are quite expensive, they are difficult to set up, calibrate, and maintain. Currently their use is limited to laboratories and studios.

In contrast RF-based techniques are attractive based on cost and ease of deployment. However traditional localization systems, such as those based on WiFi or BLE, are unreliable due to multipath effects. Ultra Wideband (UWB) radios are designed specifically to mitigate multipath reflections by utilizing short pulses rather than continuous wave RF signals.

Recently a number of researchers have reported successfully coupling UWB ranging radios with flight control electronics for vehicle state estimation, replacing or augmenting GPS as the referential system.

As early as 2011, [3] modified a MAV with a UWB localization system for indoor operation. The UWB technology investigated, by Ubisense, is based on a combination of Angle of Arrival (AOA) and Time Difference of Arrival (TDOA), where the location of the small transmitting tag is solved using time differences to static synchronized receivers. This architecture is primarily targeted at tracking large numbers of slow moving assets and requires extensive survey of each anchor location and angle plus precision calibration of the sync cables stretched between anchors.

While the UWB signalling basis provided excellent multipath resistance for indoor operation, and the small tag size allowed easy integration onto the flight vehicle, the ground-based location solver exhibited too much latency except for very slow manoeuvres.

In order to overcome these latency and anchor calibration issues recent investigations have turned toward UWB systems supporting Two-Way Ranging (TWR) rather than TDOA architectures. TWR UWB enables real-time fusion of vehicle-initiated distance measures to anchors at known coordinate locations. These range measurements can instantly be fused into the vehicle's location state estimator.

More recently [4] reported results from fusing UWB TWR measurements for aiding quadrotor state estimation. In this setup a radio mounted on a quadrotor iteratively measured distances to a

set of anchor modules at known fixed positions. This combination of UWB absolute ranges integrated with on-board accelerometers and rate gyroscopes enabled closed-loop control during agile manoeuvres. This study is especially important because they were able to measure dynamic performance using a passive motion capture (Flying Machine Arena) setup.

Although the system worked well, with UWB update rates adequate for fast manoeuvres, the results indicated *bias errors* on the order of a few centimeters from the UWB ranging system, based on Decawave DW1000 modules. These bias errors can be attributed to a combination of clock drift and multipath-induced signal strength variations, well documented in [5]. Alternatively, variations in relative antenna orientation have been shown to change pulse shape due to changes in phase delay across the multitude of frequencies contained in the pulse [ref UWB antennas]. These changes in pulse shape can lead to range bias variations, especially in 3D localization systems.

In order to counter these bias variation effects [6] used a combination of antenna diversity and multiple frequencies. In this system a location solution is determined from a full combination of 27 UWB range measurements each a combination of three mobile antennas, three anchor antennas, and three RF channels. After gathering a collection of 27 range measurements each anchor averages a 10th percentile cluster and transmits this to a basestation for localisation through a non-linear least squares approach. These solutions can then be transmitted back to the vehicle for position control. The system produced median errors around half a meter.

Although this system directly addresses antenna problems in 3D localization through antenna diversity, it suffers from scalability limitations and extended latency due to basestation-based localization estimation. This could be improved through solving location on the vehicle, and using antennas with better phase delay characteristics.

Alternatively [7] integrated a higher precision UWB ranging radio, and developed a UAV navigation system utilizing fused data from multiple aiding sources including UWB ranging, GPS, downward-facing camera, and onboard MEMS sensors. The state estimate was solved onboard a companion processor. The choice of navigation sensor combination is based on sensor availability and online sensor error estimates. An optical motion capture system was used to characterize errors through dynamic manoeuvres. GPS was simulated during the motion capture experiments.

They recognized that fusing UWB anchors with GPS requires mapping the local UWB anchor locations to GPS coordinates. They developed a novel initialization method, which takes advantage of the local accuracy afforded by downward-facing camera on a ground target. During low altitude initialization manoeuvres the optimal UWB anchor locations were estimated in the GPS system.

As a final recent example of UWB aiding for multirotor systems, [8] provides an extensive evaluation of UWB Two-Way Ranging for quadrotor navigation. While this investigation and [7] also used high precision UWB ranging radios, they used a loosely-coupled navigator, where UWB-only is used in an outer position control loop with an inner IMU attitude control loop. They excised UWB ranging outliers, attributed to transient NLOS blockages in forest flight experiments, using the Mahalanobis distance (innovation) normalized by measurement covariance. They carefully calibrated the UWB range measurements bias and standard deviations using a look up table consisting of three regions: 0 to 1.5 m subject to RF saturation, a linear LOS region from 1.5 to 50 m, and the region from 50 m onward, which experienced higher standard deviations due to Fresnel-induced ground reflections. Using this methodology they verified x-y errors indoors of 0.071 m compared to an optical motion tracking system.

They also found Extended Kalman Filter (EKF) to outperform Unscented Kalman Filter (UKF) estimation for range-based localization. They attributed this to the lack of nonlinearities in vehicle motion model. Only the measurement update, in which (polar) UWB ranging measurements are applied to motion in Cartesian system, requires linearization. In addition the UKF solution was found to yield inconsistent estimates due to the sensitivity of sigma point weights for different anchor configurations.

This paper builds upon these results, focusing specifically on UWB considerations and error sources. Primary contributions include:

- a) Autosurvey: utilizes precise anchor-to-anchor ranges with well-defined manual inputs to define the local coordinate system.
- b) Range outlier rejection: using pulse scan signature in addition to innovation-based techniques.
- c) Geometric Dilution of Precision: instantaneous accuracy estimate similar to that provided by GPS.
- d) Error sources: an analysis of significant contributions to error in an indoor 3D UAV navigation.

PULSED ULTRA WIDEBAND

This section provides an overview of the importance of short-pulse, high bandwidth signalling as a basis for localization in an environment with high multipath. These pulses are combined into packets for radio-to-radio transmissions and these packets are paired in Two-Way Ranging (TWR) conversations to support distance measurements.

Short Pulses and Multipath

The accuracy of TWR measurement depends on the receiving radio measuring the precise time of arrival (TOA) of the incoming signal. Short pulse UWB uses a signalling basis designed to reduce the effect of environmental reflections on the (TOA) measurement. The wider the bandwidth of the pulse in frequency, the shorter the pulse in time. At theoretical extremes an infinite bandwidth would produce a true impulse signal, and a single frequency would produce an unmodulated sinusoid.

Outdoors and in open space with very few reflective surfaces, there can be very little difference in TOA accuracy based on the bandwidth of the pulse. However when reflective surfaces are nearby they can have significant effects on the measurement quality.

Consider the RF channel analysis depicted in figure 2, derived from [9]. Figure 2a depicts a pulse with 1.8 GHz bandwidth centered at 4 GHz, very similar to the signalling basis of the radio used in these experiments. This signal energy occupies about 1 nanosecond of time and about 1 foot of distance.

Figure 2b depicts an alternative pulse, with the same 4 GHz center, but constrained to 80 GHz frequency bandwidth. Figure 2c illustrates the effects of a simple line-of-sight channel model with 3 reflectors within 2 meters of the direct path line between antennas. Channel effects provide the receiver with delayed and (often) inverted copies of the basis signal. The ultra-short time / ultra-wide frequency signal provides separation between the direct and reflective paths, while this same channel model, when convolved with the much narrower bandwidth basis, causes severe self-destructive interference which would make it very difficult, even with pulse compression techniques, for the receiver to accurately detect the direct path time of arrival.

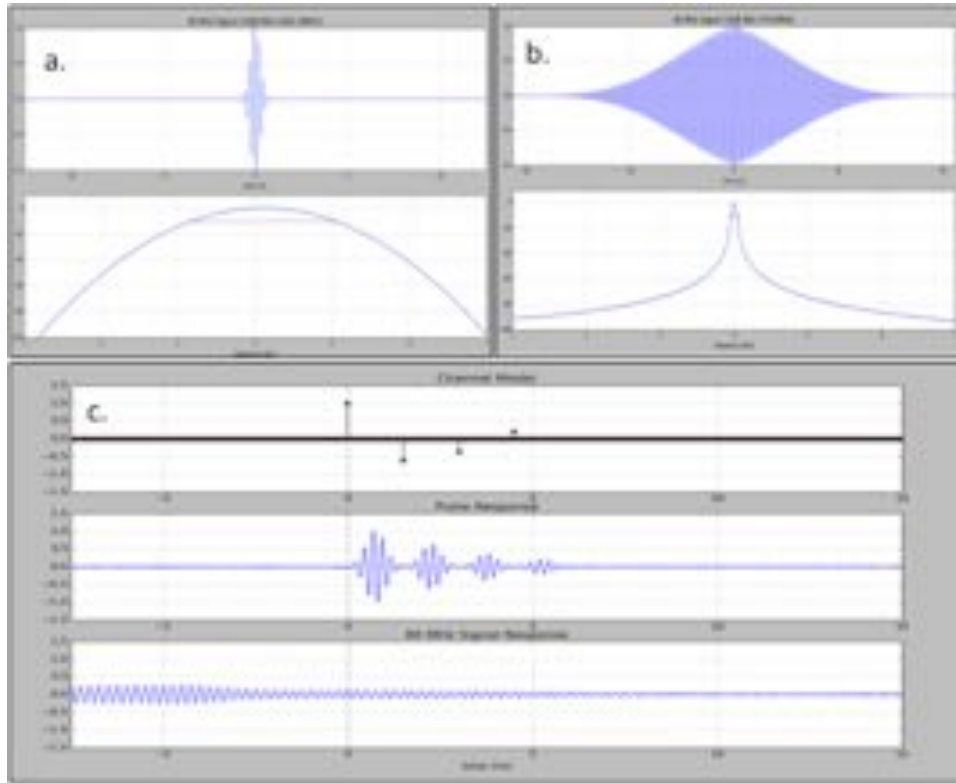


Fig. 2. Channel Impulse Response analysis of 1.8 GHz and 80 MHz pulses.
2a. Time and frequency plot of 1.8 GHz pulse. 2b. Time and frequency plot of 80 MHz pulse.
2c. Channel model with response of the two signal bases.

This relationship between bandwidth and multipath mitigation is well established in radar distance measuring systems [11] as

$$\Delta R = \frac{c}{2B} \tag{1}$$

Where ΔR is the range resolution, c is the speed of light, and B is the signal bandwidth. Using this metric a signal with 1.8 GHz bandwidth provides 22.5 times better range resolution and multipath rejection than a signal with 80 MHz bandwidth. Or, said a different way, reflective surfaces can be 22.5 times closer without significant degradation in distance measurement accuracy.

Two-Way Ranging

A single pulse, at regulated power levels, will not have nearly enough energy to travel very far before it's overcome by receiver noise. In practice a stream of pulses are transmitted and summed together to produce an image of the average pulse signature. This stream of pulses is structured into a packet, with acquisition and payload frames.

In a Two Way Ranging (TWR), one radio (the “requester”) initiates a conversation by sending a request packet including the target (“responder”) ID as data in the payload section. The responder acquires the packet, demodulates the data, scans the pulse signature and estimates the time of arrival of the pulse.

At this point the responder simply knows when the pulse arrived, based on its own time reference; it has no idea when it was sent. At a very precise time delay, relative to the request packet arrival time, the responder transmits and response packet, targeted at the requester. The requester likewise acquires, demodulates, and scans the response packet, and measures its arrival time. At this point the requester has all the information required to measure the distance. The timeline of these events are illustrated in figure 3, however the illustration simplifies the story by representing entire packets as single pulses.

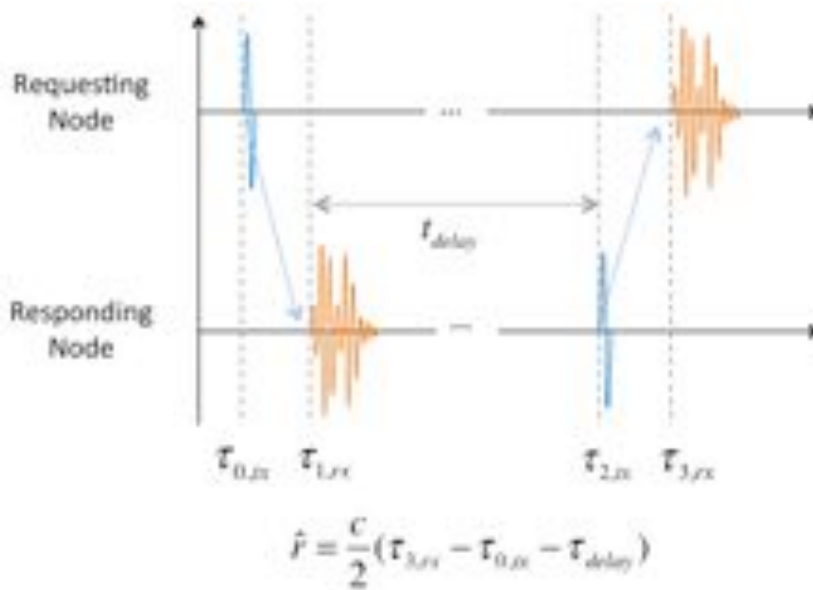


Figure 3. The time progression of a pulsed Two-Way Ranging (TWR) conversation.

In a multirotor navigation system the requesting radio is typically mounted on the vehicle and multiple responding radios are statically positioned on the ground around a coverage volume. The vehicle iteratively requests ranges from the anchors. The anchors must simply be powered and ready to respond.

LOCALIZATION

Two of the most common types of trilateration solvers are Nonlinear Least Squares (NLS) and recursive optimal (Kalman) filters. A NLS can provide higher accuracy when the radios are static, or moving slowly relative to the measurement rate. A recursive Kalman formulation is preferred when the vehicle is in motion, as it updates based on individual anchor measurements without relying on previous anchor measurements, whose latency can induce error.

Two types of NLS formulations are used, one for Extended Kalman Filter (EKF) initialization, and the other for anchor Autosurvey.

Nonlinear Least Squares for EKF Initialization

The EKF is a recursive algorithm, requiring an initial location estimate. EKF is faster to converge when its initial location is reasonably correct. Nonlinear Least Squares (NLS) using Gauss-Newton method [11] provides a straightforward means of solving for the x, y, z location based on the distances to four or more anchors at known locations. It can be used at the beginning of a flight as well as for re-initialization (“rebirth”) when the Kalman localizer fails.

In its general form the initialization NLS can be expressed as

$$P_k = \min_{(x,y,z)} \sum_{i=1}^n [\hat{r}_i^2 - (x - x_i^a)^2 + (y - y_i^a)^2 + (z - z_i^a)^2] \quad (2)$$

where:

P_k is the mobile position at time k ,

\hat{r}_i is the range measurement from vehicle to anchor i ,

x , y , and z (without subscripts) denote are the vehicle coordinates (to be computed), and

x_i^a , y_i^a , z_i^a represent the coordinates of anchor i .

Thus for a four-anchor system (the minimum required for unambiguous 3D location) the NLS initialization process involves minimization of four simultaneous equations to find three unknowns x , y , and z . The complete formulation entails derivation of derivative, or gradient equations and iteratively solving until a minimum is reached. Assuming the vehicle is initially inside the anchor box, the centroid of the anchors can be used as an initial value for this initialization.

Nonlinear Least Squares for Anchor Autosurvey

The Autosurvey NLS is a bit more elaborate, with many choices for solved dimensions. For a 3D system at least four anchors are required, with one anchor outside the plane of the other three in order to provide an unambiguous vehicle solution. Thus Autosurvey entails forming a consistent 3D polygon formed by the anchors as nodes and the links between anchors as edges, and placing this polygon on a coordinate graph.

This general system has a total of 12 unknowns: the x , y , z coordinates of the 4 anchor locations. In practice the z heights are fairly easy to manually measure from a common ground plane so these are entered as constants.

In addition, the local referential system is somewhat arbitrary; the polygon can be translated and rotated after in order to move the origin and aspect as needed by the user. Thus if one of the anchors is defined to be at the x - y plane origin and another along the x -axis (its y value assigned to zero) then this constrains the system to five unknowns for regression by the system of six equations.

Specifically the following NLS minimization involves finding a vector of five unknowns $P_A = [x_1, x_2, x_3, y_2, y_3]$ given $[\bar{x}_0, \bar{y}_0, \bar{y}_1] = [0, 0, 0]$ and manually measured $\bar{z}_i, i = 0 \dots 3$.

$$P_A = \min_{(x_1, x_2, x_3, y_2, y_3)} \left\{ \begin{array}{l} \hat{r}_{0,1}^2 - (\bar{x}_0 - x_1)^2 + (\bar{y}_0 - \bar{y}_1)^2 + (\bar{z}_0 - \bar{z}_1)^2 \\ \hat{r}_{0,2}^2 - (\bar{x}_0 - x_2)^2 + (\bar{y}_0 - y_2)^2 + (\bar{z}_0 - \bar{z}_2)^2 \\ \hat{r}_{0,3}^2 - (\bar{x}_0 - x_3)^2 + (\bar{y}_0 - y_3)^2 + (\bar{z}_0 - \bar{z}_3)^2 \\ \hat{r}_{1,2}^2 - (x_1 - x_2)^2 + (\bar{y}_1 - y_2)^2 + (\bar{z}_1 - \bar{z}_2)^2 \\ \hat{r}_{1,3}^2 - (x_1 - x_3)^2 + (\bar{y}_1 - y_3)^2 + (\bar{z}_1 - \bar{z}_3)^2 \\ \hat{r}_{2,3}^2 - (x_2 - x_3)^2 + (y_2 - y_3)^2 + (\bar{z}_2 - \bar{z}_3)^2 \end{array} \right\} \quad (3)$$

In practice, since the anchor nodes are static, many NLS solutions may be averaged for improved accuracy and variance estimation. Using a simple recursive filter updated with each new range measurement at time k , the weight α ; $0 < \alpha < 1$ is tuned for accuracy versus fast response:

$$P_{f,k} = \alpha P_{f,k-1} + (1 - \alpha) P_k \quad (4)$$

Further, at each update, the residual difference between the instantaneous and filtered solutions decreases to a minimum dictated by ranging error. This residual δP_f can provide a convenient metric of the amount of systemic bias that will be introduced in the vehicle localization solution due to anchor survey error.

$$\delta P_f = |P_{f,k+1} - P_{f,k}| \quad (5)$$

Extended Kalman Filter

An Extended Kalman Filter (EKF) is used for localization after initialization by NLS while adequate anchor geometry is available, checked by GDOP. The EKF is a formulation derived from range-only radar systems [12]. The EKF recursively maintains a state vector with six variables and a 6x6 covariance matrix. It can be divided into two parts: motion prediction and measurement update.

The prediction step simply propagates the current vehicle state estimate $\hat{\mathbf{x}}_{k-1}$ to the *a priori* estimate $\hat{\mathbf{x}}_k^-$ based on a straight-line motion model using the time since last update Δt . It also adjusts the *a priori* belief distribution \mathbf{P}_k^- using process variance σ_a^2 , set by the user. It produces the *a priori* state estimate

$$\hat{\mathbf{x}}_k^- = \mathbf{F}_{k-1}(\Delta t)\hat{\mathbf{x}}_{k-1} \quad (6)$$

$$\mathbf{P}_k^- = \mathbf{F}_{k-1}(\Delta t)\mathbf{P}_{k-1}\mathbf{F}_{k-1}^T + \mathbf{Q}_{k-1}(\Delta t, \sigma_a^2) \quad (7)$$

The measurement update begins by generating a range measurement prediction based on the position components of the *a priori* state $\hat{\mathbf{p}}_k^-$ and the anchor location p_a . This prediction is used to update the linearized measurement matrix \mathbf{H} broken into dimensional components x, y, z .

$$\hat{r}_k = \|\hat{\mathbf{p}}_k^- - p_a\| \quad (8)$$

$$\mathbf{H}_k = \left[\frac{\hat{x}_k^- - x^a}{\hat{r}_k}, 0, \frac{\hat{y}_k^- - y^a}{\hat{r}_k}, 0, \frac{\hat{z}_k^- - z^a}{\hat{r}_k}, 0 \right] \quad (9)$$

This sets up computation of the Kalman gain.

$$\mathbf{K}_k = \mathbf{P}_k^- \mathbf{H}_k^T (\mathbf{H}_k \mathbf{P}_k^- \mathbf{H}_k^T + \sigma_{r,k}^2)^{-1} \quad (10)$$

Where $\sigma_{r,k}^2$ denotes the range measurement variance at time k , determined through pulse signature analysis [13].

Using the Kalman gain the new *a posteriori* state $\hat{\mathbf{x}}_k$ and covariance \mathbf{P}_k can now be calculated using the actual UWB range measurement r_k .

$$\hat{\mathbf{x}}_k = \hat{\mathbf{x}}_k^- + \mathbf{K}_k(r_k - \hat{r}_k) \quad (11)$$

$$\mathbf{P}_k = (\mathbf{I} - \mathbf{K}_k \mathbf{H}_k) \mathbf{P}_k^- \quad (12)$$

Outlier Rejection

Range measurements are most accurate when the direct path of the RF pulse is unblocked. When the direct path is totally blocked and strong reflective paths are present (as is often the case indoors) the distance will be incorrectly calculated based on the time of flight of the first available path other than the direct path. These outliers are rejected the range variance estimated by the radio from the incoming pulse signature σ_r^2 combined with the Mahalanobis distance [12].

Specifically, the Mahalanobis distance d_m is calculated as the innovation normalized by the measurement covariance.

$$d_m = (r_k - \hat{r}_k)^2 (\mathbf{H}_k \mathbf{P}_k^- \mathbf{H}_k^T + \sigma_{r,k}^2)^{-1} \quad (13)$$

When d_m is greater than a threshold the range measurement is rejected and the filter reverts to its previous state.

Geometric Dilution of Precision

The EKF will produce locations even if there is inadequate anchor support. Geometric Dilution of Precision (GDOP) is a common metric used in GNSS receivers to assess the adequacy of the number and relative dimensional geometry of the available anchor locations. This metric is also similarly useful for UWB TWR localization systems. The UWB TWR GDOP equation is similar to that of GNSS [refPrinciples of Satellite Positioning] but without time dilation.

Assuming four anchors, the distance from the current vehicle position to each satellite is first computed.

$$r_i = \|\hat{p} - p_i^a\|, \quad i = 0,1,2,3 \quad (14)$$

These values are used to create the matrix of unit vectors from the mobile to the anchors. Here the estimated mobile location is denoted $(\hat{x}, \hat{y}, \hat{z})$ and the anchor locations $(\hat{x}_i, \hat{y}_i, \hat{z}_i), i = \{0,1,2,3\}$.

$$A = \begin{bmatrix} (\hat{x} - x_0)/r_0 & (\hat{y} - y_0)/r_0 & (\hat{z} - z_0)/r_0 \\ (\hat{x} - x_1)/r_1 & (\hat{y} - y_1)/r_1 & (\hat{z} - z_1)/r_1 \\ (\hat{x} - x_2)/r_2 & (\hat{y} - y_2)/r_2 & (\hat{z} - z_2)/r_2 \\ (\hat{x} - x_3)/r_3 & (\hat{y} - y_3)/r_3 & (\hat{z} - z_3)/r_3 \end{bmatrix} \quad (15)$$

The geometric covariance matrix Q is formed from the generalized inverse of this matrix with identity weighting.

$$Q = (A^T A)^{-1} = \begin{bmatrix} \sigma_x^2 & \sigma_{xy}^2 & \sigma_{xz}^2 \\ \sigma_{xy}^2 & \sigma_y^2 & \sigma_{yz}^2 \\ \sigma_{xz}^2 & \sigma_{yz}^2 & \sigma_z^2 \end{bmatrix} \quad (16)$$

The diagonal elements of Q provide estimates of the error expansion in the Cartesian dimensions. The total GDOP estimate is the square root of the trace of Q .

$$GDOP = \sqrt{\text{tr}(Q)} \quad (17)$$

GDOP is an estimate of the expansion of localization error with respect to the underlying ranging error. GDOP will be close to 1 in the center of the 3D geometry of the anchors. As the mobile recedes from the center position its localization will increase. A calculated GDOP of (e.g.) 4 implies the location error is 4 times that of the underlying measurement error. If the running anchor list drops below three anchors the A matrix will become singular and the inversion to Q will fail, implying “infinite” 3D localization error. When GDOP exceeds a predefined threshold the vehicle transitions into safe mode.

AUTOSURVEY SETUP AND OPERATION

Four anchor nodes were placed on tripods and the heights of their antennas were measured using a hand-held laser range finder. The anchors were then placed in an ad-hoc system similar to the one shown in figure 4a. The basestation that runs the Autosurvey GUI is attached to an arbi-

bitrary anchor node. Figure 4b shows spatial separation in the Z Axis needed to provide angular diversity for improved 3D localization performance.

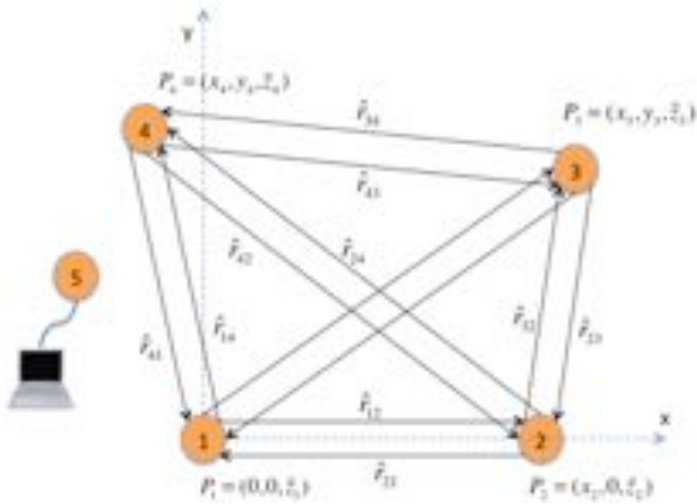


Figure 4a. Example system of four ad-hoc anchor nodes and connected basestation with GUI.

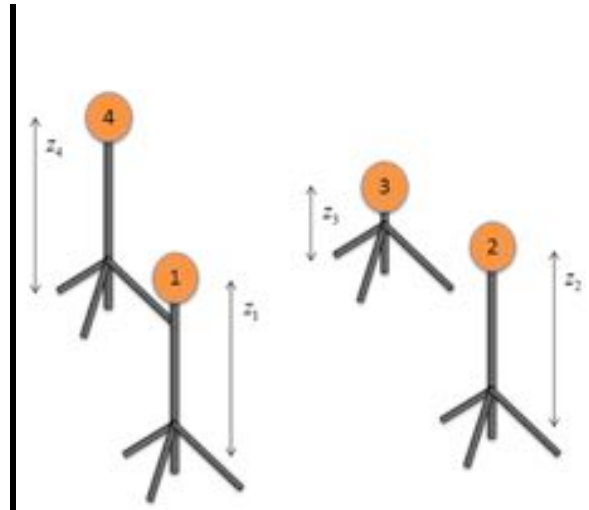


Figure 4b. Example of spatial diversity in the Z Axis for 3D localization.

A Location Map (LMAP) is defined with the basestation GUI. The LMAP serves two primary purposes; first to define the role of a node in the overall tracking system and second to constrain the anchors to a quadrant of the Cartesian coordinate system. A representation of the LMAP is shown in Table 1. To constrain an anchor for the definition of the coordinate system, an anchor is classified as either an Origin anchor, +\X Axis anchor, or +\Y Axis anchor. Any additional anchors participating in Autosurvey are classified as ‘Anchors’.

The LMAP also contains the initial and fixed coordinates of the anchors. The initial coordinates are used as initial conditions to seed the WNLS algorithm and the fixed coordinates define the anchors role in the coordinate system. The initial coordinates are shown in the LMAP in the shaded cells and the fixed are unshaded.

Once the LMAP is defined the basestation GUI will load it into the node it is connected to. That node in turn will broadcast out the LMAP so that all nodes participating in Autosurvey will hear the broadcast and load the LMAP into their configuration. Those nodes will send an acknowledgement to the basestation GUI so the user is ensured the LMAP was received by all the anchors.

Table 1. The Location Map for the Autosurvey phase of operation

#	Node ID	Type	ELR	X(mm)	Y (mm)	Z (mm)
1	100	Origin	yes	0	0	2500
2	101	+X Axis	yes	1000	0	2500
3	102	+Y Axis	yes	0	1000	2500

4	103	Anchor	yes	1000	1000	2500
5	104	Mobile	yes	500	500	1000

Once the LMAP has been loaded into all participating nodes, the basestation GUI will instruct the nodes to go into an Autosurvey mode. This will cause only the anchor nodes to start ranging to each other per an implementation of the ALOHA network protocol. The anchors will use a random hold-off time for sending range requests and subsequently range to all the other anchors in a round-robin fashion.

As indicated in the LMAP all nodes were configured with Echo Last Range (ELR) enabled. ELR instructs the node to include its previous range measurement in the next range request packet transmission. The node connected to the basestation GUI will hear the range request packet and pull out the range measurement. It sends it to the basestation GUI which makes the range measurement available to the NLS algorithm as described previously.

After the map residual falls to a minimum the basestation GUI commands the nodes to idle mode and loads the results of the Autosurvey into the LMAP, replacing the initial coordinates. As before, the basestation GUI broadcasts the new LMAP to all nodes in the system.

FLIGHT EXPERIMENT

The quadrotor localization test was performed indoors with four anchor radios mounted on tripods distributed in four corners of a lobby with approximately 6x6x10m volume as shown in figure 5. Three of the anchor radios were elevated to 2.31m while the fourth was lowered to 1.63m off the common ground plane as measured to the center of each antenna element.



Figure 5. Indoor test area with anchor setup

A 3D Robotics DIY Quad with Pixhawk flight controller as shown in figure 6 was used as the flight platform. A P440 UWB radio from Time Domain [REFTIMEDOMAIN] was mounted on top, with extended connection to a downward-facing PulsON Broadspec antenna. The dipole antenna was pointed down in order to minimize direct-path blockage while above the anchor plane.

A Mini-Circuits 15542 VHF-3100+ high-pass filter was placed inline between the radio and the antenna element due to increased noise detected in the pulse waveform, isolated to the antenna input during motor acceleration. 12V battery power to the radio was conditioned using a custom LC filter (typically used for video noise reduction) with inline 100uH inductor and parallel 16V, 470uF capacitor.



Figure 6. Quadrotor platform with P440 UWB radio

The estimated flight path solution, with indicated flight path, is provided in figure 7. The jaggy patterns are due to a combination of survey and bias error, enhanced as the vehicle transitioned through the approximate anchor plane. Lack of anchor diversity in the z-axis caused this visible increase in error. This is especially indicated in the GDOP analysis below.

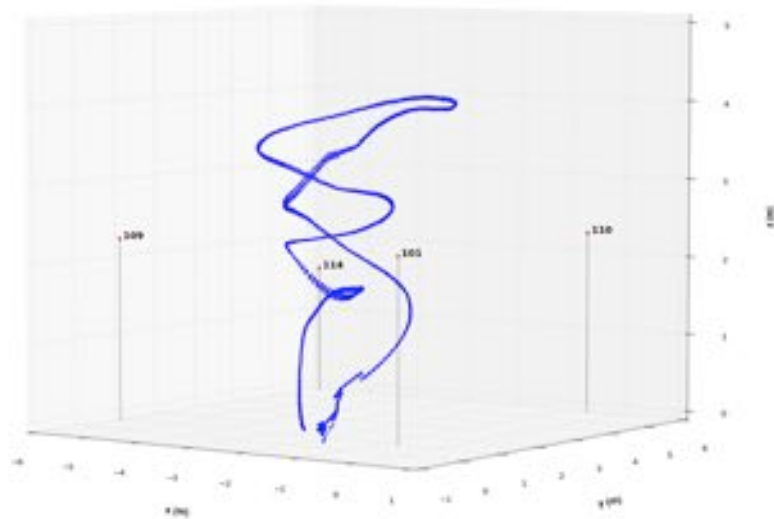


Figure 7. An isometric view of estimated flight path.

The raw ranges were clean (static tests show less than 2 cm range error at the anchor centroid) except for a couple of outliers each to anchor 101 and 110 during take-off where the vehicle's arms partially blocked the direct path. These errors were detected and removed by the outlier

detection process described previously.

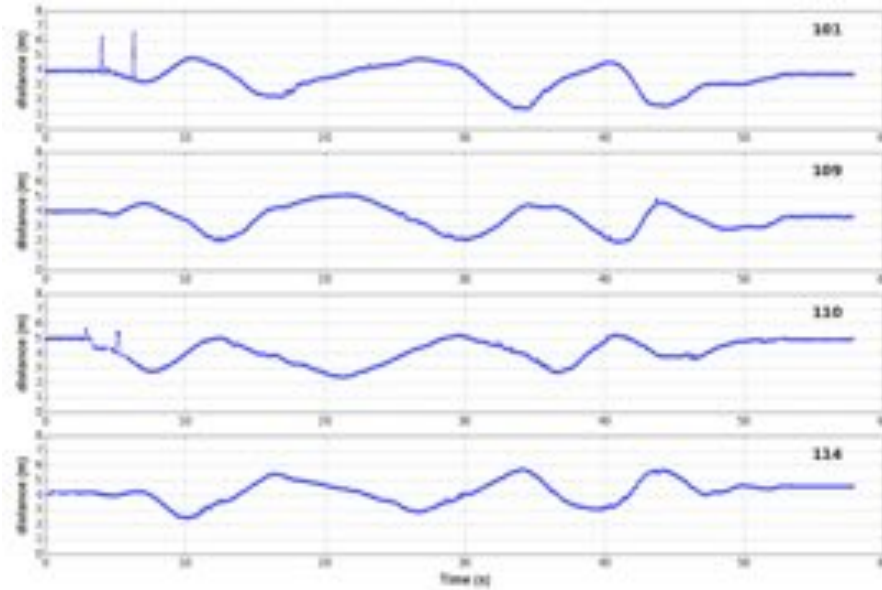


Figure 8. Raw range measurements versus time from each of the four anchors.

Individual, x , y , and z solutions to the EKF state are provided in figure 9. Note a slight increase in variation of the z values 15 and 45 seconds into the test as the vehicle transitioned through the anchor centroid region.

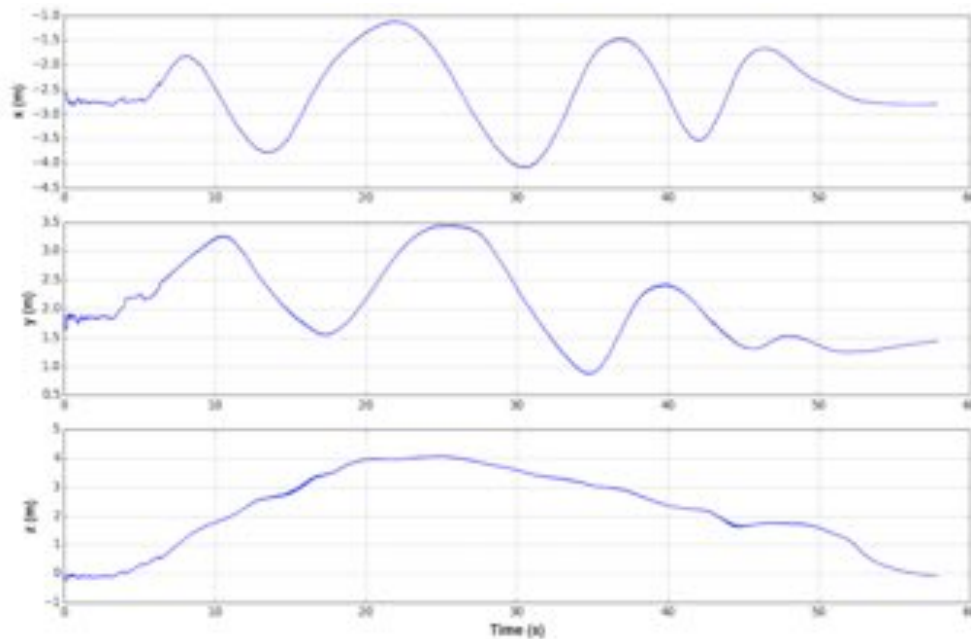


Figure 9. Time progression of x , y , and z coordinate solutions throughout the experiment.

The EKF variance estimates are provided in Figure 10. Note the growth in z variance during transition through the antenna plane. Even with NLS initialization the EKF requires approximately 5 seconds to settle. This indicates the initial covariance could be reduced for faster set-

ting time.

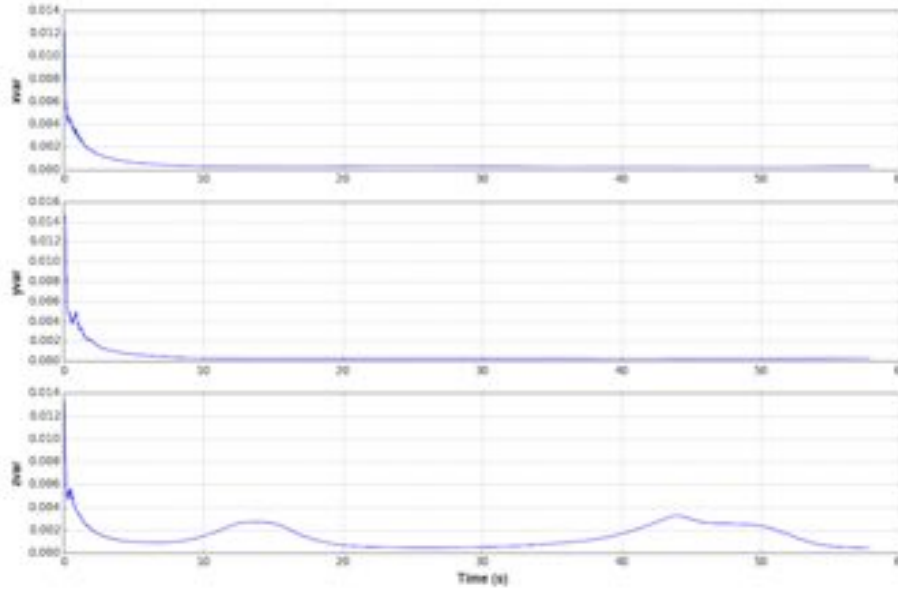


Figure 10. Time progression of the variance estimates of x, y, and z.

As a final experimental result figure 11 provides the progression of GDOP as well as its dimensional components through the flight. The two large spikes during take-off and landing, as the vehicle transitioned through the anchor box, are almost entirely due to dilution of precision in the z-height axis. Although anchor 114 was lower than the others by 0.7 m, this provides an excellent indication that this was inadequate, especially compared to the ~5 m separation in x and y dimensions.

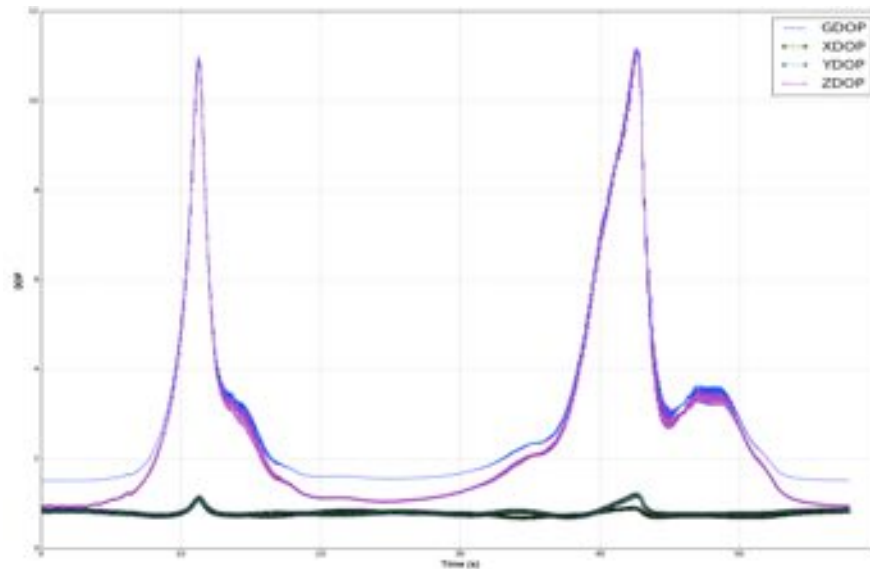


Figure 11. Comparison of GDOP, xdop, ydop, and zdop throughout the flight test.

DISCUSSION

All measurement systems have error. We estimated a maximum total 3D error less than 10 cm throughout the flight experiment, with maximum occurring during transition through the region with poor z-axis geometry. In general this system has five major sources of error:

Range Measurement Error

The UWB TWR measurement in line of sight conditions has statistical errors on the order of a centimeter. Slight bias variations, on the order of a centimeter, can be caused due to variations in group delay, especially in the elevation dimension of a UWB dipole antenna. This variation in frequency alignment causes changing pulse shape. This, combined with partial blockage of direct path by the vehicle itself, or indoor obstacles, can cause bias changes of a few centimeters. Total blockage of the direct path can Range Error consists of two types of error: bias and variance (aka. systemic and statistical, aka. mean and standard deviation.) In ideal conditions both of these are less than 2 cm on P440. Many things can increase this error such as saturation, NLOS, RF interference, etc.

Geometric Dilution of Precision

While this isn't actually an error source, this phenomenon is often the most significant component to error in localization systems which otherwise have good line-of-sight anchor coverage. GDOP amplifies the range error when forming a 2D or 3D solution. The GDOP metric is minimal (GDOP=1.0) when the tracked location is in an ideal central location in the middle of the anchor geometry. Anywhere else in the volume, the GDOP will expand, reflecting a expansion of localization error in a cross-axis relative to the direction of the the anchor centroid.

Anchor Survey Error

The localization solver combines distance measurements to anchors at "known locations" to update the mobile location. Errors in these surveyed locations will manifest in the navigation solution as bias error in the range measurements. Bias errors will cause offset in the location or, given a round-robin ranging network, off-track jags during flight towards or away from the miss-located anchor.

Latency and Acceleration Error

The solver computes a new location with each new range measurement. If the mobile is moving faster than the system update rate can support then the mobile solution will appear "behind" its true location.

Related to the previous, the solver blends each range measurement in a filter. This filter averages ranges together with assumed constant velocity. When acceleration occurs the EKF requires an extended number of measurements to realign its intrinsic velocity estimate. Acceleration can take the form of speeding up, stopping, or changing course left or right. A quick reversal of forward motion is an easy way to induce the most acceleration on the mobile. This error takes the form "overshoot". The process noise parameter of the EKF can be adjusted to balance acceleration error with the smoothness of the straight-line path solution.

Introduction of acceleration measurements in the Kalman state can reduce the acceleration error without inducing latency.

CONCLUSION

This experiment shows that ranging radios with 1.8 GHz pulse bandwidth provide an excellent replacement to GNSS for indoor navigation of a multicopter. Solution errors were found to be

less than 10 cm in the worst case, when z-axis diversity was at its minimum, and less than 2cm otherwise. The Autosurvey technique allowed fast and accurate deployment of anchor radios. EKF localization with NLS initialization provides an accurate real time 3D localization system. Outliers due to direct path blockage can be removed using the Mahalanobis distance metric, augmented with the range error estimate intrinsic to the radios tested.

The GDOP metric, common in GNSS systems, is straightforward to implement and has low computational cost for real time calculation. It provides an excellent tool for real-time safety assessment, and post-processing analysis of the suitability of anchor geometry.

Future work includes integrating the local navigation solutions into the flight control and path guidance systems, integrating inertial aiding, and testing various antenna and anchor configurations with improved outlier rejection.

REFERENCES

- [1] S. Lupashin, M. Hehn, M. W. Mueller, A. P. Schoellig, M. Sherback, and R. D'Andrea, A platform for aerial robotics research and demonstration: The Flying Machine Arena, *Mechatronics*, Volume 24, Issue 1, February 2014, Pages 41-54
- [2] N. Michael, D. Mellinger, Q. Lindsey and V. Kumar, "The GRASP Multiple Micro-UAV Testbed," in *IEEE Robotics & Automation Magazine*, vol. 17, no. 3, pp. 56-65, Sept. 2010.
- [3] B. Watts, Integration of control algorithms for quadrotor UAV's using an indoor sensor environment. M. S. Thesis, Naval Postgraduate School, Monterey, CA, 2011.
- [4] M. Mueller, M. Hamer, and R. D'Andrea, R, Fusing ultra-wideband range measurements with accelerometers and rate gyroscopes for quadcopter state estimation, *IEEE International Conference on Robotics and Automation (ICRA)*, Seattle, WA, May 26-30, 2015.
- [5] Decawave, Application Note APS011, Sources of Error in DW1000 based two-way ranging schemes, v1.0 2014 pp.10-14.
- [6] B. Kempke, P. Pannuto, and P. Dutta, "PolyPoint: Guiding Indoor Quadrotors with Ultra-Wideband Localization." In Proc. 2nd International Workshop on Hot Topics in Wireless. Hot-Wireless@MobiCom 2015.
- [7] K. Hausman, S. Weiss, R. Brockers, L. Matthies and G. S. Sukhatme. "Self-Calibrating Multi-Sensor Fusion with Probabilistic Measurement Validation for Seamless Sensor Switching on a UAV". To appear in *2016 International Conference on Robotics and Automation (ICRA 2016)*, May 2016.
- [8] K. Guo et. al., "Ultra-Wideband-Based Localization for Quadcopter Navigation," *Unmanned Systems 2016* 04:01, pp. 23-34.
- [9] A. F. Molisch et. al., IEEE 802.15.4a channel model - final report, *Converging: Technology, work and learning*. Australian Government Printing Service, 2004.
- [10] M. Skolnik, *Introduction to Radar Systems*, Tata McGraw Hill, 2001.
- [11] J. Nocedal and S. Wright. *Numerical optimization*. New York: Springer, 1999.
- [12] Y. Bar-Shalom, X. Rong Li, and T. Kirubarajan, *Estimation with Applications to Tracking and Navigation*, New York: John Wiley & Sons 2002, pp. 381-394.
- [13] B. Dewberry and W. Beeler, "Increased ranging capacity using Ultrawideband direct-path

pulse signal strength with dynamic recalibration," *Position Location and Navigation Symposium (PLANS), 2012 IEEE/ION*, Myrtle Beach, SC, 2012, pp. 1013-1017.